

Article

Synthesis and Thermoelectric Properties of TiO₂/Cu₂SnSe₃ Composites

Jiai Ning, Di Wu and Degang Zhao *

School of Materials Science and Engineering, University of Jinan, Jinan 250022, China; crystal4885@sina.com (J.N.); 18366100143@163.com (D.W.)

* Correspondence: mse_zhaodg@ujn.eu.cn; Tel.: +86-531-8276-7561

Received: 1 September 2017; Accepted: 10 October 2017; Published: 12 October 2017

Abstract: Thermoelectric (TE) materials are a kind of energy material which can directly convert waste heat into electricity based on TE effects. Ternary Cu₂SnSe₃ material with diamond-like structure has become one of the potential TE materials due to its low thermal conductivity and adjustable electrical conductivity. In this study, the Cu₂SnSe₃ powder was prepared by vacuum melting-quenching-annealing-grinding process. The nano-TiO₂ particles were introduced into the Cu₂SnSe₃ matrix by ball milling. Spark plasma sintering (SPS) was employed to fabricate the TiO₂/Cu₂SnSe₃ composites. The X-ray diffraction (XRD), field emission scanning electron microscopy (FE-SEM), and transmission electron microscopy (TEM) were used to study the phase and microstructure of TiO₂/Cu₂SnSe₃ composites. Electrical resistivity, Seebeck coefficient, and thermal conductivity measurement were applied to analyze the thermoelectric properties. For the 1.4%TiO₂/Cu₂SnSe₃ composite, the electrical conductivity was improved whereas the Seebeck coefficient was lower than that of pure Cu₂SnSe₃. For other TiO₂/Cu₂SnSe₃ samples, the Seebeck coefficient was improved while the electrical conductivity was reduced. The thermal conductivity of TiO₂/Cu₂SnSe₃ composites was lower than that of Cu₂SnSe₃ matrix, which is attributed to the lower carrier conductivity. A maximum ZT of 0.30 at 700 K for the 1.0%TiO₂/Cu₂SnSe₃ composite was obtained, which was 17% higher than that of the pure Cu₂SnSe₃ at 700 K.

Keywords: thermoelectric; Cu₂SnSe₃; nano-TiO₂; composites

1. Introduction

Humans need to care for our “mother earth” with intelligence, diligence, and heart. In a society experiencing an energy shortage, the pursuit of sustainable development has become the social mainstream. With rapid economic development, industrial scale expands. However, energy and environmental problems gradually appear at the same time. In the process of industrial production, most energy is released in the form of heat. Thermoelectric (TE) materials can directly convert waste heat into electricity based on the Seebeck effect [1,2]. While TE materials show a great prospect environmentally and economically, the lower efficiency of TE materials limits their wide application. The efficiency of TE materials is determined by the dimensionless figure of merit ZT , which is defined as $ZT = \alpha^2 \sigma T / \kappa$, where α is Seebeck coefficient, σ is electrical conductivity, κ is the thermal conductivity, and T is absolute temperature. A good TE material should have high α and σ as well as low κ value. The intrinsic properties of TE materials determine the coupling effect between the conductivity and Seebeck coefficient. Generally, the higher power factor ($PF = \alpha^2 \sigma$) corresponds to higher power output. PF is proportional to the effect mass (m^*) and mobility of the carriers (μ). Thermal property is determined by the total thermal conductivity (κ), which is composed of lattice part (κ_L) and carrier part (κ_e). Electronic thermal conductivity (κ_e) is proportional to the conductivity. Reducing the κ_L of a TE material is an effective way to reduce the total thermal conductivity.

Cu_2SnSe_3 with a diamond structure has gained great attention recently due to its low thermal conductivity originating from the complex crystal structure and high specific heat. In addition, Cu_2SnSe_3 has good electrical conductivity and adjustable electrical properties [3]. To further improve the thermoelectric properties of Cu_2SnSe_3 , a great deal of research has been carried out to optimize the material from multiple perspectives. Li et al. obtained a maximum ZT of 0.45 for Cu_2SnSe_3 material at 773 K by one-step high-pressure combustion synthesis (HPCS) [4]. Liu et al. prepared the Cu_2SnSe_3 material using combustion synthesis and obtained a maximum ZT of 0.51 at 773 K, which is the best result for Cu_2SnSe_3 compared to other methods [5]. Wang et al. optimized the synthesis parameters to form uniform particles of wurtzite, cubic, linear heterostructures, and tetrapods by colloidal synthesis. The facile synthesis strategy opens pathways for extension to other compositions of multielement copper chalcogenides where the cubic and hexagonal phases can be formed [6]. Ge et al. and Ahmadi et al. synthesized Cu_2SnSe_3 nanocrystals and controlled the nanostructure successfully by solvothermal method [7,8]. In addition to optimizing the preparation process, doping of materials is also an important way to enhance the performance of TE materials. Cho et al. synthesized a Ga-doped $\text{Cu}_2\text{Ga}_{1-x}\text{Ge}_x\text{Se}_3$ sample and approached its theoretical minimum value of lattice thermal conductivity, resulting in a ZT value of 0.5 at 750 K [9]. Fan et al. reported a lower lattice thermal conductivity of the $\text{Cu}_2\text{Ga}_{0.075}\text{Sn}_{0.925}\text{Se}_3$ sample and obtained a maximum ZT of 0.43 at 700 K [10]. In addition, Skoug et al. confirmed that substituting Se with S is also an effective method to improve the TE performance of Cu-based ternary selenides [11]. The combustion synthesis method can prepare high-performance thermoelectric materials, but it is difficult to precisely control. Moreover, many studies report that only Sn location is the best candidate for substituting in the $\text{Cu}_2\text{Sn}(\text{Ge})\text{Se}(\text{S})_3$ structure, which limits the improvement of TE performance [3,8,10]. Based on those limits mentioned above, the composite was designed on the Cu-based ternary selenides matrix. Some studies confirmed that introducing a nanophase into the Cu-based semiconductor can improve the ZT . Zhang et al. introduced graphite nanosheets into CuGaTe_2 and obtained the highest ZT of 0.93 for the CuGaTe_2 composite at 873 K, which is 21% higher than that of CuGaTe_2 matrix [12]. Li et al. reported that the incorporation of a suitable quantity of nanophase PbTe particles into SnSe matrix could efficiently enhance the TE performance of SnSe material [13]. TiO_2 has a band gap of 3.0 eV and has good thermal and chemical stability as well as large elastic modulus, which makes it a good candidate as a second phase. TiO_2 has been introduced into a filled-skutterudite matrix in previous studies [14–16]. However, introducing nano- TiO_2 into Cu_2SnSe_3 has never been reported. In this study, the technological parameter was optimized to synthesize pure Cu_2SnSe_3 material. The nano- TiO_2 was incorporated into the Cu_2SnSe_3 matrix by ball milling method, and the $\text{TiO}_2/\text{Cu}_2\text{SnSe}_3$ thermoelectric composites were prepared by spark plasma sintering (SPS). The thermoelectric properties of $\text{TiO}_2/\text{Cu}_2\text{SnSe}_3$ composites were investigated in detail.

2. Experimental Procedures

2.1. Materials Synthesis

In order to ensure a desirable Cu_2SnSe_3 compound, elementary powders of Cu (powder, 99.99%), Sn (powder, 99.99%), and Se (shot, 99.99%, Sinopharm Chemical Reagent Co., Ltd., Shanghai, China) were weighted accurately to the atomic ratio of Cu_2SnSe_3 . Then, the powders were mixed in an agate mortar with ethyl alcohol and dried in vacuum drier at 350 K. Next, the powder mixture was loaded into a graphite crucible, which was sealed in a quartz ampoule under vacuum. After the above steps were completed, the quartz ampoule was put in a vertical furnace heated slowly to 1273 K and held for 12 h, followed by cooling with different rates (samples 1–3). Then, some thus-obtained samples were annealed at 923 K for three days (sample 4). Finally, the ingots (sample 1–4) were ground into fine powder in an agate mortar.

Commercial nano- TiO_2 powder (average particle size: 7 nm, 99.8%, Shanghai Chemical Industry Park Co., Shanghai, China) was incorporated into the Cu_2SnSe_3 powder by ball milling in an argon

atmosphere at volume fractions of 0.5, 1.0, 1.4, and 1.8 vol %, respectively. The TiO₂/Cu₂SnSe₃ composite powder was obtained in a planetary mill at 300 rpm for 180 min. The weight ratio of balls to powders was about 10:1. The TiO₂/Cu₂SnSe₃ composite powders were densified by spark plasma sintering (SPS 2040) in graphite die (10 mm in diameter) at around 740 K for about 8 min under uniaxial pressure of 50 MPa in vacuum.

2.2. Phase, Structural Characterizations, and Transport Property

The densities of all the TiO₂/Cu₂SnSe₃ composite samples were measured by Archimedes method. The constituent phases can be detected by X-ray diffractometry (Cu K_α, D8-Advance, Bruker Corporation, Karlsruhe, Germany). The microstructure was characterized by field emission scanning electron microscopy (FESEM, QUANTA 250 FEG, ThermoFisher Scientific, Hillsboro, OR, USA) on polished and fractured samples. Transmission electron microscope (TEM) observations were performed on a JEM-2010 instrument (JEOL, Tokyo, Japan) with the voltage of 200 KV. The electrical conductivity and Seebeck coefficient were measured simultaneously using commercial equipment (ZEM-3, ULVAC-RIKO, Tokyo, Japan). The Hall coefficient (R_H) was measured using the van der Pauw's method in vacuum with the magnetic field of 2 T. The carrier concentration (p_H) and mobility (μ_H) were estimated from the relations of $p_H = 1/(eR_H)$ and $\mu_H = \sigma R_H$ based on the assumption of single band model, where e is the electronic charge. The thermal conductivity can be calculated by using the follow equation:

$$\kappa = C_p \times d \times \lambda \quad (1)$$

where C_p , d , and λ are specific heat, density, and thermal diffusivity, respectively. The thermal diffusivity was measured by a laser flash technique (LFA427, Netzsch, Wunsiedel, Germany) in a flowing Ar atmosphere. Specific heat was measured from room temperature to 700 K in argon using a differential scanning calorimeter (DSC1-1600HT, STA 409, Netzsch, Wunsiedel, Germany). All the measurements were performed in a temperature range of 300–700 K. All the measurements of thermoelectric properties were carried out three times to ensure the accuracy of ZT value.

3. Results and Discussion

Figure 1a shows the XRD patterns of the resultant Cu₂SnSe₃ samples after melting and annealing with different cooling rates. Samples 1 and 2 were cooled from 1273 K to room temperature in 24 h and 48 h, respectively. Sample 3 was directly quenched in salt water. Sample 4 was annealed at 923 K for 24 h after quenching in salt water. The XRD patterns indicate that Cu₂SnSe₃ can be synthesized by melting at 1273 K for 12 h and annealing. The Cu₂SnSe₃ matrix is a disordered zincblende structure with a lattice parameter of 5.684 Å. Figure 1b shows the XRD patterns of different samples from 10° to 40°. There was no significant difference between sample 1 and sample 2, while the sample 4 had fewer peaks, which may be indexed to the monoclinic structure [3]. The structure transformation in Cu₂SnSe₃ from monoclinic to cubic can be attributed to the different cooling rates. Skoug reported that slow cooling could result in a monoclinic structure while water quenching led to a disordered cubic zincblende-like structure [17]. Delgado et al. reported that an order–disorder transformation in Cu₂SnSe₃ can occur at 723 K and the modified phase was found to be sphalerite [18]. In order to comprehensively and thoroughly study these phases, Marcano et al. found that the phase in low diffraction position was likely to be SnSe₂ on the basis of differential thermal analysis (DTA) [19]. Therefore, the structure of Cu₂SnSe₃ can be described as an adamantane compound which is derivative of the sphalerite structure. In this study, the Cu₂SnSe₃ material prepared by the melting, quenching, and annealing process was selected as the matrix phase (sample 4) to carry out the following experiment.

The Cu₂SnSe₃ bulk ingot was artificially ground into powder, as shown in Figure 2a. It can be seen that the size distribution of Cu₂SnSe₃ particles is not uniform. In order to obtain smaller uniform particles, the powder was subjected to mechanical ball milling, and the SEM image of Cu₂SnSe₃ powder after ball milling is shown in Figure 2b. The XRD of Cu₂SnSe₃ matrix was analyzed before

and after ball milling, as shown in Figure 3. There was no phase change reaction in the process of ball milling of Cu_2SnSe_3 matrix.

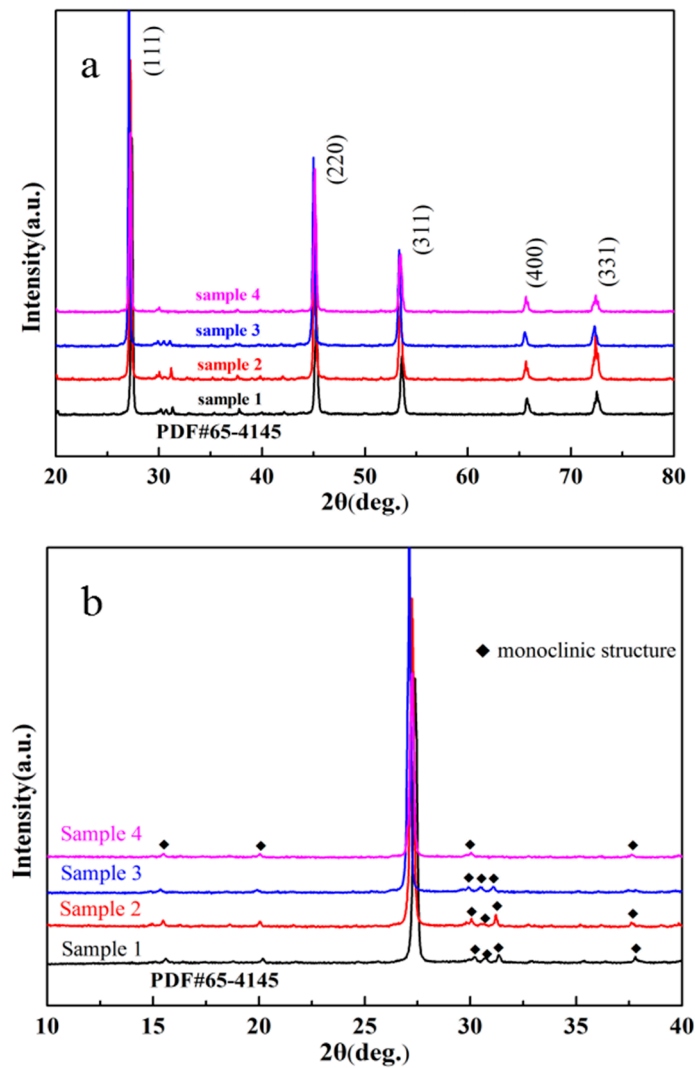


Figure 1. The X-ray diffraction (XRD) patterns of Cu_2SnSe_3 powders with different cooling rates: (a) from 20° to 80° ; (b) amplified XRD patterns from 10° to 40° . Samples 1–3 correspond to Cu_2SnSe_3 samples with different cooling rates and sample 4 corresponds to the annealed Cu_2SnSe_3 sample.

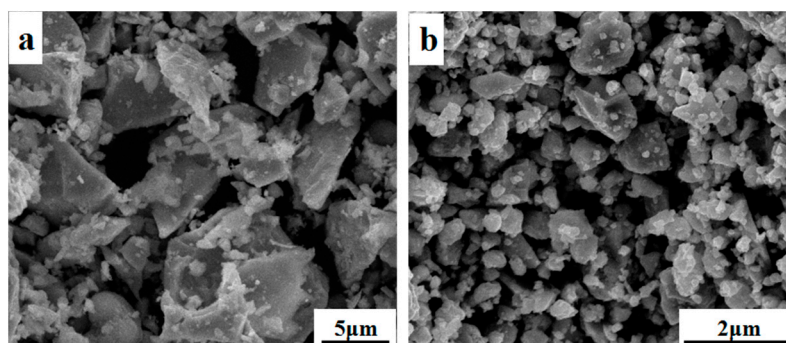


Figure 2. SEM images of Cu_2SnSe_3 powder: (a) before ball milling; (b) after ball milling.

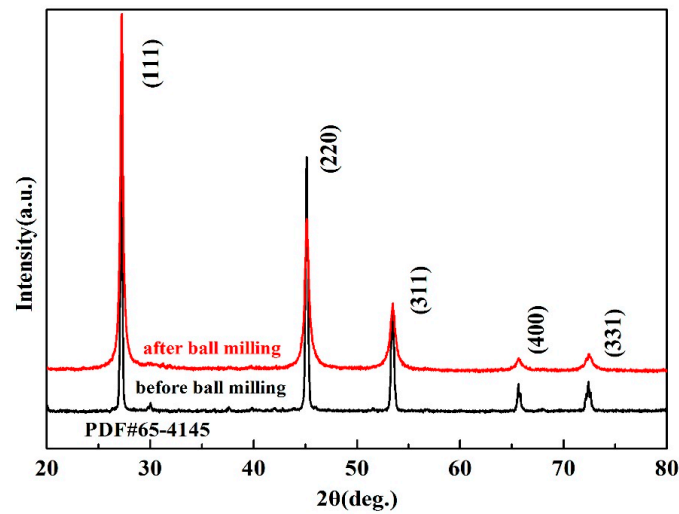


Figure 3. The XRD patterns of Cu_2SnSe_3 powder before and after ball milling.

Figure 4 shows the XRD patterns of x vol % $\text{TiO}_2/\text{Cu}_2\text{SnSe}_3$ ($x = 0, 0.6, 1.0, 1.4, 1.8$) composites after ball-milling. The XRD patterns of composites samples are similar to that of Cu_2SnSe_3 matrix samples. The diffraction peaks of all the samples correspond to the Cu_2SnSe_3 phase (PDF#65-4145). The peak of TiO_2 phase is hardly found in the XRD patterns, which may be attributed to its low content. In addition, no diffraction peaks corresponding to other phase was found, which indicates that there was no reaction between the introduced nano- TiO_2 particles and the Cu_2SnSe_3 matrix in the process of ball-milling. Figure 5a shows the TEM image of the starting powders of TiO_2 nanoparticles. It is shown that the size of spherical TiO_2 particles is 10–20 nm. Figure 5b–f shows the SEM images of the fracture surface of $\text{TiO}_2/\text{Cu}_2\text{SnSe}_3$ composite samples. It can be observed in Figure 5b that the grain size of Cu_2SnSe_3 matrix is about 3 μm . Rapid sintering process with SPS technology can effectively inhibit the growth of grains, which would result in more grain boundaries and scatter more phonons. It also can be found in Figure 5c,d, and f that the nano- TiO_2 particles are mainly distributed on the grain boundary. With the content of nano- TiO_2 increasing from 0.6 vol % to 1.8 vol %, the grain size of Cu_2SnSe_3 decreases from 2.2 μm to 0.9 μm . The nano- TiO_2 particles in the sintering process effectively inhibited the growth of grains, and the inhibitory effect is more obvious with the increase of nanoparticles [20–22]. In contrast, it can be found in Figure 5e that most TiO_2 particles in the 1.4% $\text{TiO}_2/\text{Cu}_2\text{SnSe}_3$ composites were distributed in the internal grain. This is possibly related to the surfactivity of powder, SPS process, and so on. This issue will be investigated in future work. In addition, when the amount of nano- TiO_2 reached 1.8 vol %, the $\text{TiO}_2/\text{Cu}_2\text{SnSe}_3$ composite kept more holes at the grain boundary. The microstructure of $\text{TiO}_2/\text{Cu}_2\text{SnSe}_3$ composites could influence the electrical and thermal transport properties of the materials. The relative density of $\text{TiO}_2/\text{Cu}_2\text{SnSe}_3$ composites is shown in Table 1. It can be seen that the addition of nano- TiO_2 reduced the relative density of $\text{TiO}_2/\text{Cu}_2\text{SnSe}_3$ composites.

Table 1. Density of the x vol % $\text{TiO}_2/\text{Cu}_2\text{SnSe}_3$ composites with different nano- TiO_2 content.

$x\text{TiO}_2/\text{Cu}_2\text{SnSe}_3$	$x = 0$	$x = 0.6$	$x = 1.0$	$x = 1.4$	$x = 1.8$
Density (g/cm^3)	6.042	6.017	5.833	5.686	5.343
Relative density	98%	97.8%	97.2%	96.5%	95.6%

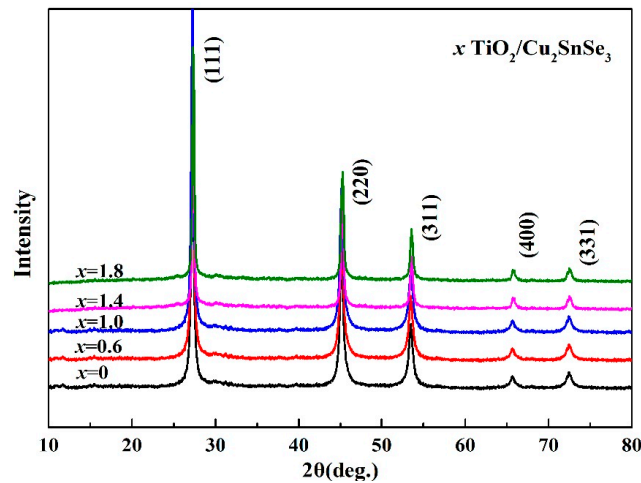


Figure 4. The XRD patterns of the x vol % $\text{TiO}_2/\text{Cu}_2\text{SnSe}_3$ composites.

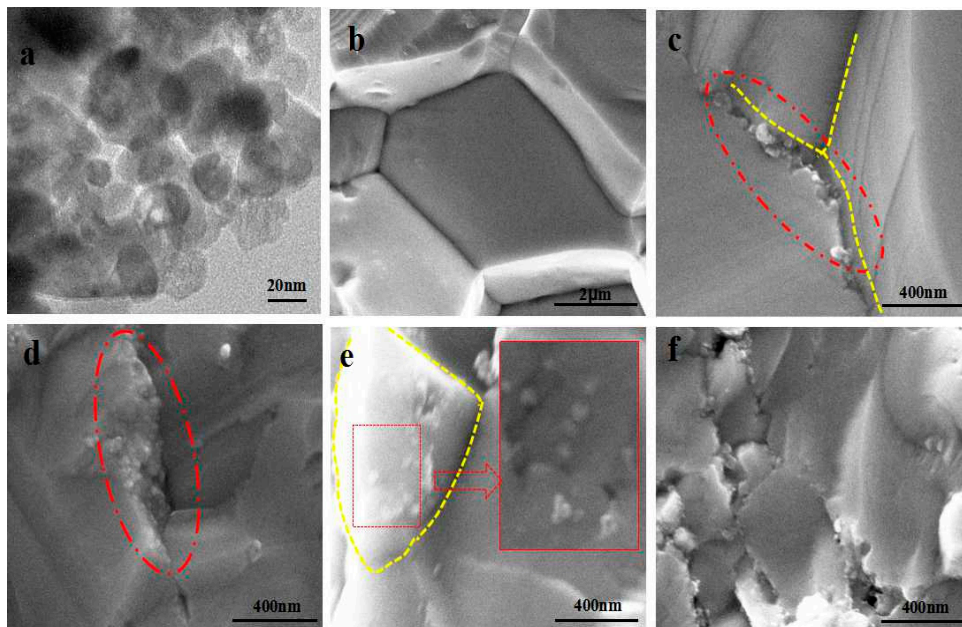


Figure 5. (a) TEM image of the initial TiO_2 nanoparticles. (b–f) SEM images of the x vol % $\text{TiO}_2/\text{Cu}_2\text{SnSe}_3$ composites: (b) $x = 0$; (c) $x = 0.6$; (d) $x = 1.0$; (e) $x = 1.4$; (f) $x = 1.8$.

Figure 6 shows the temperature dependence of electrical conductivity (σ) for the $\text{TiO}_2/\text{Cu}_2\text{SnSe}_3$ composites in the range of 300–700 K. The electrical conductivity of all samples decreased with increasing temperature in all of the investigated temperatures, which indicates that all samples demonstrated degenerate semiconductor behavior. The composites samples showed lower σ than the Cu_2SnSe_3 matrix except for the 1.4% $\text{TiO}_2/\text{Cu}_2\text{SnSe}_3$ sample, which suggests that the addition of nano- TiO_2 into the Cu_2SnSe_3 matrix can reduce the electrical conductivity. Nano- TiO_2 particles affect the carrier transport, leading to a reduction in the conductivity of the material. On the other hand, the nano- TiO_2 particles which were distributed at the grain boundary effectively suppressed the grain growth, resulting in a large number of grain boundaries during the sintering process. These grain boundaries have great effects on the transport of the carriers, which reduce the conductivity of the material. However, the conductivity of the 1.4% $\text{TiO}_2/\text{Cu}_2\text{SnSe}_3$ sample was effectively improved. As shown in Figure 5e, the nano- TiO_2 particles in the 1.4% $\text{TiO}_2/\text{Cu}_2\text{SnSe}_3$ composites were mainly

distributed in the internal grain. Therefore the effect of suppressing the grain growth was not as obvious as that of other composites. Meanwhile, the carrier concentration of 1.4%TiO₂/Cu₂SnSe₃ composite at room temperature is listed in Table 2. The increase in the conductivity of the 1.4%TiO₂/Cu₂SnSe₃ composite is attributed to the high carrier mobility. These nanoparticles distributed in the grain provide a special channel and contribute to the transport for the carrier. The electrical conductivity of 1.4%TiO₂/Cu₂SnSe₃ sample was $2.91 \times 10^3 \Omega^{-1}/\text{cm}$ at room temperature. Compared with the electrical conductivity of doped-Cu₂SnSe₃ sample in the previous studies [8–11], the electrical conductivity of TiO₂/Cu₂SnSe₃ sample was higher, which is possibly due to high carrier concentration (about 10^{21} cm^{-3}), as shown in Table 2.

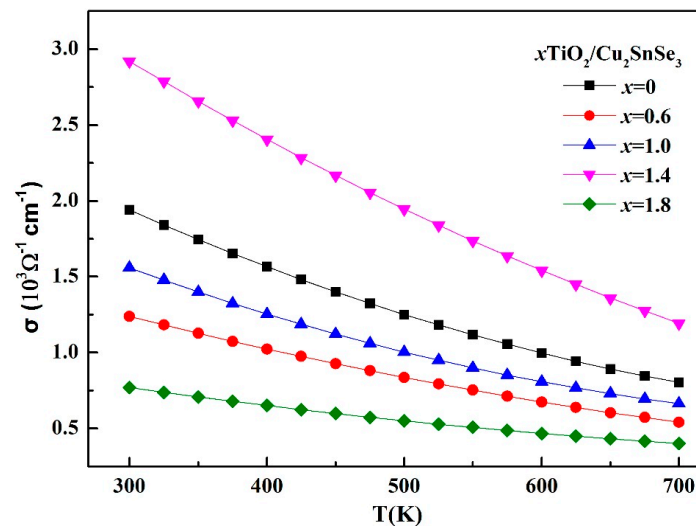


Figure 6. Temperature dependence of electrical conductivity for the TiO₂/Cu₂SnSe₃ composites.

Table 2. The physical parameters of the x vol % TiO₂/Cu₂SnSe₃ composite at room temperature.

$x\text{TiO}_2/\text{Cu}_2\text{SnSe}_3$	$R_H (10^{-3} \text{ cm}^3/\text{C})$	$p (\text{cm}^{-3})$	$\mu (\text{cm}^2/\text{Vs})$	$\sigma (10^3 \Omega^{-1}/\text{cm})$
$x = 0$	3.368	1.86×10^{21}	6.58	1.96
$x = 0.6$	3.621	1.71×10^{21}	4.61	1.25
$x = 1.0$	3.262	1.92×10^{21}	5.38	1.64
$x = 1.4$	3.570	1.75×10^{21}	10.4	2.91
$x = 1.8$	3.31	1.89×10^{21}	2.54	0.77

Figure 7 shows the temperature dependence of Seebeck coefficient (α) of the TiO₂/Cu₂SnSe₃ composite samples. All samples kept positive values of α in the whole temperature range, indicating that they are *p*-type semiconductors. The Seebeck coefficient of all samples increased with increasing temperature. The Seebeck coefficient of all samples was higher than that of the matrix material, except for the 1.4%TiO₂/Cu₂SnSe₃ sample. The introduction of nano-TiO₂ brings a large number of phase interfaces, which can filter out the low-energy carriers so as to increase the density of states of the material. As a result, the Seebeck coefficient of composites was improved. As for the 1.4%TiO₂/Cu₂SnSe₃ sample, the lower Seebeck coefficient should be related with the different distribution of nano-TiO₂ particles in the TiO₂/Cu₂SnSe₃ composite. Combined with the above analysis of the microstructure and conductivity, there is an effective channel in the composite which allows a large number of low-energy carriers to pass through, so the composite maintains a lower Seebeck coefficient. The detailed reason will be further investigated. Figure 8 shows the temperature dependence of the power factor (PF) of the TiO₂/Cu₂SnSe₃ composites. The PF of 1.4%TiO₂/Cu₂SnSe₃ reached $5.27 \times 10^{-4} \text{ Wm}^{-1} \text{ K}^{-2}$ at 700 K, which is 20% higher than that of Cu₂SnSe₃ matrix material ($4.59 \times 10^{-4} \text{ Wm}^{-1} \text{ K}^{-2}$). For the other TiO₂/Cu₂SnSe₃ composites, since the increase in the Seebeck

coefficient is not sufficient to compensate for the decrease in conductivity, the PF of the composite samples is maintained at a lower level than that of the Cu_2SnSe_3 matrix.

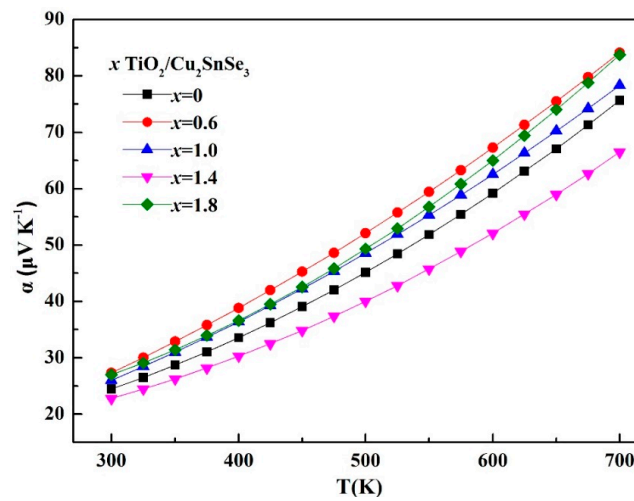


Figure 7. Temperature dependence of Seebeck coefficient for the $\text{TiO}_2/\text{Cu}_2\text{SnSe}_3$ composites.

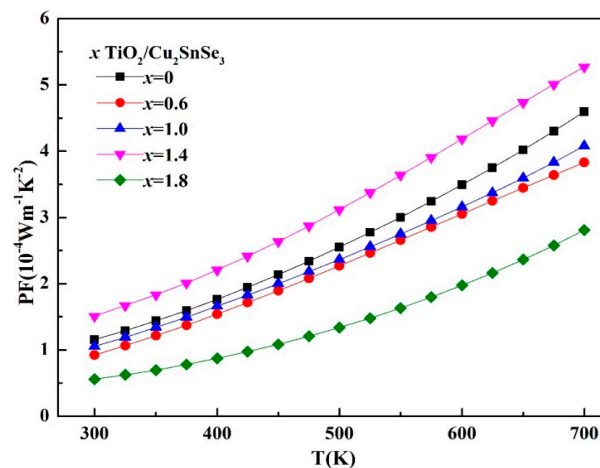


Figure 8. Temperature dependence of power factor (PF) for the $\text{TiO}_2/\text{Cu}_2\text{SnSe}_3$ composites.

Figure 9 shows the temperature dependence of thermal conductivity (κ) of the $\text{TiO}_2/\text{Cu}_2\text{SnSe}_3$ composite. Compared with the κ of Cu_2SnSe_3 matrix, it can be seen in Figure 9a that the $\text{TiO}_2/\text{Cu}_2\text{SnSe}_3$ composites maintained the lower κ , except for the 1.4% $\text{TiO}_2/\text{Cu}_2\text{SnSe}_3$ sample. The 1.4% $\text{TiO}_2/\text{Cu}_2\text{SnSe}_3$ composite kept higher κ than that of the Cu_2SnSe_3 matrix. The lattice thermal conductivity (κ_L) of the $\text{TiO}_2/\text{Cu}_2\text{SnSe}_3$ composite can be calculated from the total thermal conductivity (κ) minus the carrier thermal conductivity κ_e ($\kappa_e = L\sigma T$), as shown in Figure 9b. It can be observed that the κ_L of 1.4% $\text{TiO}_2/\text{Cu}_2\text{SnSe}_3$ sample was significantly reduced before 450 K. The higher κ of 1.4% $\text{TiO}_2/\text{Cu}_2\text{SnSe}_3$ in the temperature of 450–700 K is mainly due to the high κ_e , which is closely related with the distribution of nano- TiO_2 phase in the internal grain. The expected decrease of κ_L due to the addition of nano- TiO_2 is not evident in other $\text{TiO}_2/\text{Cu}_2\text{SnSe}_3$ composites, which is possibly attributed to the distribution of nano- TiO_2 in the grain boundaries. However, the κ_L of 1.4% $\text{TiO}_2/\text{Cu}_2\text{SnSe}_3$ sample is 1.43 W/mK at room temperature, which is now the lowest value of lattice conductivity for Cu_2SnSe_3 sample and obviously lower than the previous studies. Fan et al. reported a lattice thermal conductivity of about 2.25 W/mK at room temperature for Ga-doped Cu_2SnSe_3 sample fabricated by hot pressing sintering [10]. Compared

with the Ga- or In-doped Cu_2SnSe_3 sample, the lower κ_L of $\text{TiO}_2/\text{Cu}_2\text{SnSe}_3$ sample in this study should be related with the distribution of TiO_2 .

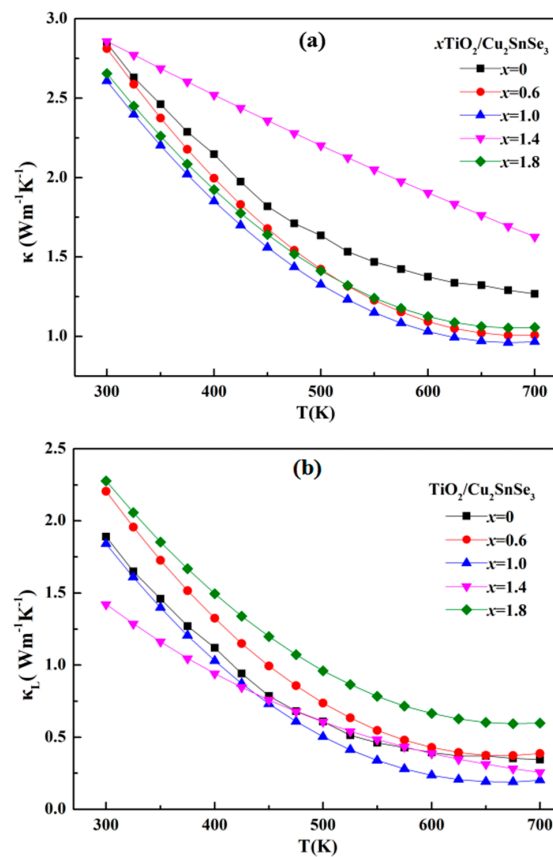


Figure 9. (a) Temperature dependence of total thermal conductivity and (b) lattice thermal conductivity for the $\text{TiO}_2/\text{Cu}_2\text{SnSe}_3$ composites.

Figure 10 shows the temperature dependence of the dimensionless figure of merit ZT of $\text{TiO}_2/\text{Cu}_2\text{SnSe}_3$ composites. It can be seen that the ZT value of 1.4% $\text{TiO}_2/\text{Cu}_2\text{SnSe}_3$ composite was not improved due to its higher κ . The maximum ZT value for 1.0% $\text{TiO}_2/\text{Cu}_2\text{SnSe}_3$ composite is 0.30 at 700 K, which is 17% higher than that of Cu_2SnSe_3 matrix.

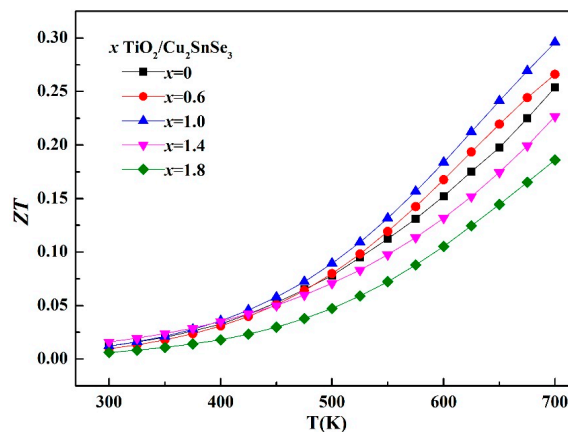


Figure 10. Temperature dependence of ZT for $\text{TiO}_2/\text{Cu}_2\text{SnSe}_3$ composites.

4. Conclusions

In this study, TiO₂/Cu₂SnSe₃ composites were prepared by melting, ball milling, and spark plasma sintering. The distribution of nano-TiO₂ in the Cu₂SnSe₃ matrix plays an important role in the thermoelectric transport properties. For the 1.4%TiO₂/Cu₂SnSe₃ composite, the nano-TiO₂ particles were mainly distributed in the internal grain, and the higher carrier mobility gave it a higher conductivity. The higher carrier thermal conductivity allowed the 1.4%TiO₂/Cu₂SnSe₃ to have a higher total thermal conductivity. For the other TiO₂/Cu₂SnSe₃ composites, the nano-TiO₂ particles were mainly distributed on the grain boundary of the Cu₂SnSe₃ matrix, and the growth of the grains was effectively inhibited. Due to the lower carrier thermal conductivity, the other TiO₂/Cu₂SnSe₃ composites had a lower total thermal conductivity. The maximum *ZT* value for 1.0%TiO₂/Cu₂SnSe₃ composite was 0.30 at 700 K, which is 17% higher than that of Cu₂SnSe₃ matrix.

Acknowledgments: The authors would like to thank the help for the measurement of TE properties in Tongji University. Financial supports from the National Natural Science Foundations of China (No. 51772132 and No. 51471076) are gratefully acknowledged.

Author Contributions: All authors participated in the research, data analysis and edition of the manuscript. Degang Zhao designed the experiments and analyzed the data. Jiai Ning performed the experiments and wrote the paper. Di Wu carried out the experimental measurement.

Conflicts of Interest: The authors declare no conflicts of interest.

References

1. Shi, X.; Chen, L.D.; Uher, C. Recent advances in high-performance bulk thermoelectric materials. *Int. Mater. Rev.* **2016**, *6*, 1–37. [[CrossRef](#)]
2. Fitriani, R.O.; Long, B.D.; Barma, M.C.; Riaz, M.; Sabri, M.F.; Said, S.M.; Saidur, R. A review on nanostructures of high temperature thermoelectric materials for waste heat recovery. *Renew. Sustain. Energy Rev.* **2016**, *64*, 635–659. [[CrossRef](#)]
3. Wubet, W.; Kuo, D.H. Structural and electrical properties of Si- and Ti-doped Cu₂SnSe₃ bulks. *J. Solid State Chem.* **2015**, *227*, 239–246. [[CrossRef](#)]
4. Li, Y.; Liu, G.; Li, J. High thermoelectric performance of In-doped Cu₂SnSe₃ prepared by fast combustion synthesis. *New J. Chem.* **2016**, *40*, 5394–5400. [[CrossRef](#)]
5. Liu, G.; Chen, K.; Li, J. Combustion synthesis of Cu₂SnSe₃ thermoelectric materials. *J. Eur. Ceram. Soc.* **2016**, *36*, 1407–1415. [[CrossRef](#)]
6. Wang, J.; Liu, P.; Seaton, C.C. Complete colloidal synthesis of Cu₂SnSe₃ nanocrystals with crystal phase and shape control. *J. Am. Chem. Soc.* **2014**, *136*, 7954–7960. [[CrossRef](#)] [[PubMed](#)]
7. Ge, Z.H.; Salvador, J.R.; Nolas, G.S. Selective Synthesis of Cu₂SnSe₃ and Cu₂SnSe₄ nanocrystals. *Inorg. Chem.* **2014**, *53*, 4445–4449. [[CrossRef](#)] [[PubMed](#)]
8. Ahmadi, M.; Pramana, S.S.; Batabyal, S.K. Synthesis of Cu₂SnSe₃ nanocrystals for solution processable photovoltaic cells. *Inorg. Chem.* **2013**, *52*, 1722–1728. [[CrossRef](#)] [[PubMed](#)]
9. Cho, J.Y.; Shi, X.; Salvador, J.R. Thermoelectric properties and investigations of low thermal conductivity in Ga-doped Cu₂GeSe₃. *Phys. Rev. B* **2011**, *84*, 085207. [[CrossRef](#)]
10. Fan, J.; Liu, H.; Shi, X. Investigation of thermoelectric properties of Cu₂Ga_xSn_{1-x}Se₃ diamond-like compounds by hot pressing and spark plasma sintering. *Acta Mater.* **2013**, *61*, 4297–4304. [[CrossRef](#)]
11. Skoug, E.J.; Cain, J.D.; Morelli, D.T. Improved thermoelectric performance in Cu-based ternary chalcogenides using S for Se substitution. *J. Electron. Mater.* **2012**, *41*, 1232–1236. [[CrossRef](#)]
12. Zhang, J.; Qin, X.; Li, D. Enhanced thermoelectric performance of CuGaTe₂ based composites incorporated with graphite nanosheets. *Appl. Phys. Lett.* **2016**, *108*, 073902. [[CrossRef](#)]
13. Li, D.; Li, J.C.; Qin, X.Y. Enhanced thermoelectric performance in SnSe based composites with PbTe nanoinclusions. *Energy* **2016**, *116*, 861–866. [[CrossRef](#)]
14. He, Z.; Stiewe, C.; Platzek, D. Effect of ceramic dispersion on thermoelectric properties of nano ZrO₂/CoSb₃ composites. *J. Appl. Phys.* **2007**, *101*, 043707. [[CrossRef](#)]
15. Zhao, X.Y.; Shi, X.; Chen, L.D. Synthesis of Yb_yCo₄Sb₁₂/Yb₂O₃ composites and their thermoelectric properties. *Appl. Phys. Lett.* **2006**, *89*, 2121. [[CrossRef](#)]

16. Chubilleau, C.; Lenoir, B.; Candolfi, C. Thermoelectric properties of $\text{In}_{0.2}\text{Co}_4\text{Sb}_{12}$ skutterudites with embedded PbTe or ZnO nanoparticles. *J. Alloys Compd.* **2014**, *589*, 513–523. [[CrossRef](#)]
17. Skoug, E.J.; Cain, J.D.; Morelli, D.T. Thermoelectric properties of the Cu_2SnSe_3 - Cu_2GeSe_3 solid solution. *J. Alloy. Compd.* **2010**, *506*, 18–21. [[CrossRef](#)]
18. Delgado, G.E.; Mora, A.J.; Marcano, G. Crystal structure refinement of the semiconducting compound Cu_2SnSe_3 from X-ray powder diffraction data. *Mater. Res. Bull.* **2003**, *38*, 1949–1955. [[CrossRef](#)]
19. Marcano, G.D.; Chalbaud, L.M.; Rincón, C. Crystal growth and structure of the semiconductor Cu_2SnSe_3 . *Mater. Lett.* **2002**, *53*, 151–154. [[CrossRef](#)]
20. Huang, X.Y.; Xu, Z.; Chen, L.D. The thermoelectric performance of $\text{ZrNiSn}/\text{ZrO}_2$ composites. *Solid State Commun.* **2004**, *130*, 181–185. [[CrossRef](#)]
21. Zhu, Y.; Shen, H.; Chen, H. Effects of nano- TiO_2 dispersion on thermoelectric properties of $\text{Co}_4\text{Sb}_{11.7}\text{Te}_{0.3}$ composites. *Rare Met.* **2012**, *31*, 43–47. [[CrossRef](#)]
22. Zhao, L.D.; Zhang, B.P.; Li, J.F. Preparation and properties of nano-SiC dispersed Bi_2Te_3 thermoelectric materials. *Rare Met. Mater. Eng.* **2007**, *36*, 408–412.



© 2017 by the authors. Licensee MDPI, Basel, Switzerland. This article is an open access article distributed under the terms and conditions of the Creative Commons Attribution (CC BY) license (<http://creativecommons.org/licenses/by/4.0/>).